Multi-Sensory System for Spatially Aware Colonoscopy

Tuukka Panula, Bruno Rosa, *Member, IEEE*, Salzitsa Anastasova-Ivanova, Matti Kaisti, and Benny Lo, *Senior Member, IEEE*

***Abstract*—The traditional method of performing a colonoscopy requires a trained physician operating the instrument manually. There is no proper feedback to aid the user in the process and typically the physician has to rely solely on the camera output to guide the endoscope. This method can lead to discomfort or even colon perforation due to the elongated endoscope scratching or tearing the colon tissue. To address this issue and enable spatial awareness to the instrument, we propose a modular multi-sensor system that integrates bending, pressure, and motion sensing units into the endoscope. All sensors are manufactured using inexpensive off-the-shelf components. The proposed sensor system was characterized on a robotic test bench and validated in a colon phantom study. The results demonstrate the feasibility and robustness of the proposed sensor fusion approach in colonoscopy which has the potential for safer and more effective inspection of the bowels. The introduction of these sensing modalities to an endoscope paves the way for AI-assisted and possibly autonomous colonoscopy in the future.**

***Index Terms*—Colonoscopy, sensor, pressure, strain, IMU.**

I. Introduction

A. Motivation

COLONOSCOPY is the gold standard method for diagnosing gastrointestinal disease, with more than one million procedures performed each year in the UK alone [1]. Although generally safe, it requires a highly trained and experienced clinician to carry out the procedure and could still lead to complications. As traditional colonoscope does not have any sensing capability, endoscopists have to rely on the camera images to navigate inside the colon and their feeling of friction when inserting the colonoscope into the lumen to avoid damages to the colon tissues. However, the elongated colonoscope, which is bent and twisted while being inserted into the large intestine, can easily scratch or tear the colon tissue, causing pain and discomfort for the patient, and could even rupture the colon wall [2]. Pain experienced during colonoscopy is usually caused by one of three reasons [3]. i) When the operator pumps CO_2 gas to insufflate the colon to allow the colonoscope to pass through the lumen and to obtain a clear view of the surrounding tissue, a portion of the colon could get overly inflated which causes pain. ii) Excessive force applied to the colon wall by the colonoscope can cause pain and, in the worst case, perforation - rupturing the colon wall. iii) In many cases, the pain experienced is due to looping, which means the colonoscope is being forced into certain shapes while inserting into the colon. Typical loop formations include the N and alpha loops [4], with names that stem from their respective shapes. It has been reported that looping occurs in 90 percent of all colonoscopies [3]. Both excessive pressure and looping can be very difficult to prevent without having any other feedback than the scope's camera view. Assistive systems have been introduced to assist endoscopic gastrointestinal surgery, especially in the form of robotic-driven platforms [5].

B. Related Work

There are devices available commercially to minimize pain and track the movement of the endoscope during the procedure. The simplest is an abdominal compression vest (Colowrap, North Carolina) that is used to prevent the colon from moving and thus the instrument from looping. However, its efficacy has been questioned [6]. ShapeLock (USGI Medical, California) is a sleeve that when placed around the colonoscope, prevents looping by restricting the curving of the instrument by locking itself to place [7]. Magnetic endoscope imaging (MEI) is a powerful technique where a set of coils are attached to the endoscope shaft at certain intervals and a detection coil is placed near the patient [8]. This way, a three-dimensional image of the instrument can be constructed to be used as an aid to the examiner in locating the endoscope tip. One such system on the market is ScopeGuide (Olympus, Japan) [9]. Magnetic manipulation of the scope tip has also been proposed in [10]. Relating academic endeavors have also been reported, such as a soft robotic sleeve that has inflatable pockets along with optical waveguides to measure contact pressure [11]. The air pockets can be inflated when excessive force is directed to the endoscope. The forces exerted in colonoscopy using sensor technology have been studied before. By placing a handle equipped with force sensors on the scope shaft, researchers were able to record the push and

Manuscript received 19 November 2024; revised 14 February 2025; accepted 7 April 2025. Date of publication 23 May 2025; date of current version 21 August 2025. This article was recommended for publication by Associate Editor F. Ficuciello and Editor P. Dario upon evaluation of the reviewers' comments. This work was supported in part by the University of Turku Graduate School (UTUGS) Grant; in part by the Instrumentarium Science Foundation, Finland; and in part by the Engineering and Physical Sciences Research Council, U.K., under Grant EP/P012779. *(Corresponding author: Tuukka Panula).*

Tuukka Panula is with the Hamlyn Centre, Imperial College London, SW7 2AZ London, U.K., and also with the Department of Computing, University of Turku, 20500 Turku, Finland (e-mail: tuukka.j.panula@utu.fi).

Bruno Rosa, Salzitsa Anastasova-Ivanova, and Benny Lo are with the Hamlyn Centre, Imperial College London, SW7 2AZ London, U.K.

Matti Kaisti is with the Department of computing, University of Turku, 20500 Turku, Finland.

Digital Object Identifier 10.1109/TMRB.2025.3573053

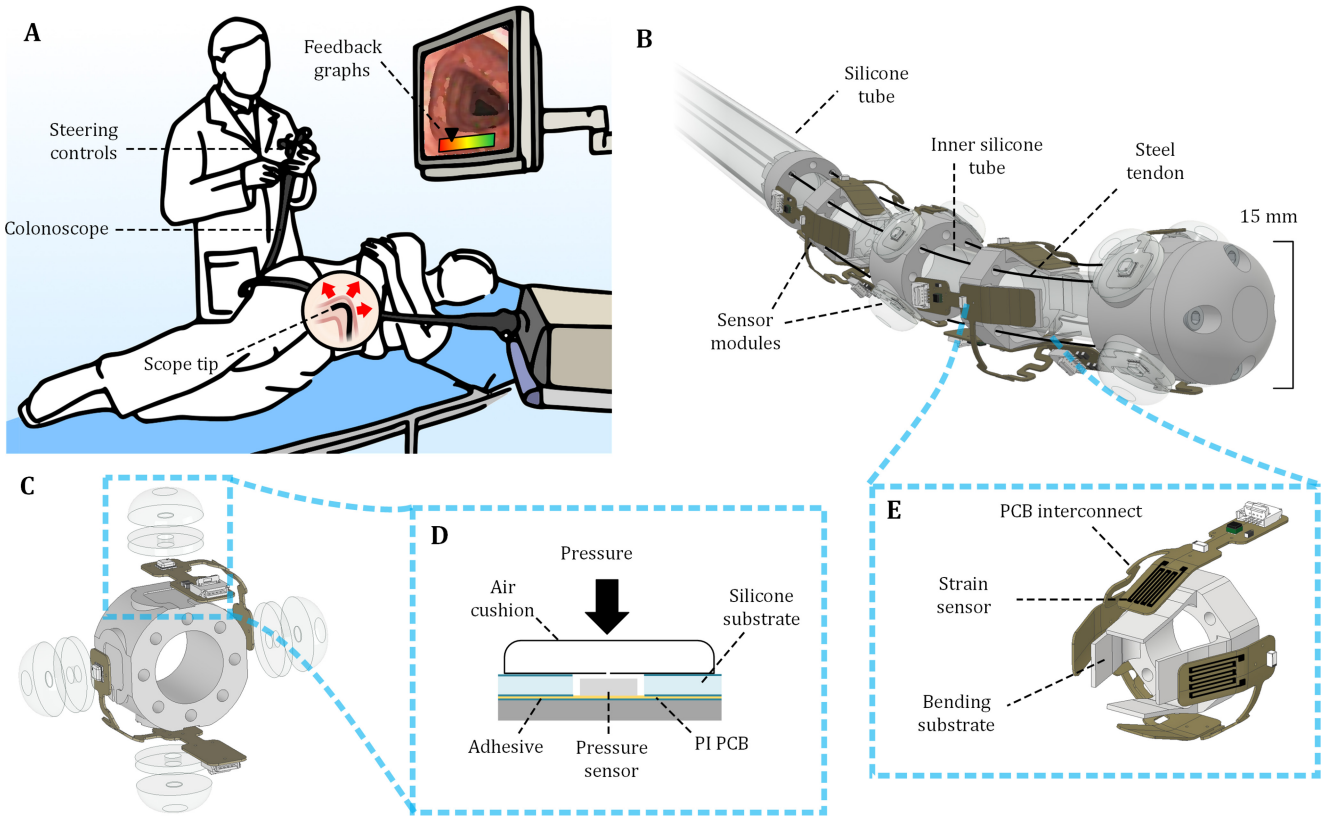

Fig. 1. Instrument overview. a) Illustration of the proposed system in use. b) 3D rendition of the flexible endoscope tip with the sensors PCBs assembled. Two different sized silicone tubes, outer and inner, are used. c) Pressure sensing module assembly. Four pressure sensors are attached in 90 degree intervals, enabling a four directional pressure profile. The proposed instrument is a dedicated system rather than a conventional colonoscope. d) Cross-section figure of a single pressure sensor module. e) Bending sensor module assembly. The sensor PCBs are attached to the substrate with the opposite sides connected together via a flexible interconnect.

pull forces during the procedure [12]. In another study, a force sensing sheath consisting of an array of conductive copper tapes was wrapped around the endoscope. By measuring the effect of applied force on their resistance, along with simultaneous MEI, the researchers could reconstruct a 3D force map of the colonoscope [13]. The use of bending sensors to detect looping have also been proposed by [14]. In this approach, the researchers attached a series of resistive bending sensors to the probe shaft, giving the examiner feedback of the probe angle. However, using only strain sensors, looping detection is very limited and only works when the loop has already formed. We believe, that by fusing sensor data from multiple different sensor modalities we can collect sufficient information to prevent looping.

Alternative directions of development in less intrusive colonoscopy are the use of untethered devices and endorobots. Capsule endoscopy is a technique where a small device equipped with cameras is ingested by the patient. While passing through the gastrointestinal system, the device sends image data to the operator [15]. Similar technology is used in a self-propelling variant [16]. In another study, a soft robotic device uses pressurized balloons to navigate through the colon [17]. Magnetic tracking technology has also been adopted to capsule endoscopy in a instrumentation setup called MagnetOFuse [18]

C. Overview

To minimize the risk of colon rupture and looping during colonoscopy, we propose a modular sensor system equipped with contact pressure and scope bending sensing, as well as a 6-axis inertial measurement unit (IMU) to allow endoscope sensing. These sensors can be used together to provide the user real-time feedback of the forces exerted to the colon wall, endoscope's orientation, and bending of each joint. Traditional endoscopes do not have any sensing modalities for receiving input from its state. In our technique, contact pressure to the lumen wall is measured via barometric pressure sensors that are covered with air cushions, using a construction similar to [19]. Bending sensing is achieved using strain gauges in a half-bridge Wheatstone bridge connected to a instrument amplifier setup [20]. The advancement of the scope is recorded by measuring the 3D orientation of the scope tip using integration and Kalman filtering, while being inserted to the colon. A 3D rendition of the proposed system is shown in Figure 1b. Consequently, the user can monitor both the tip of the scope and the proximal portion of the shaft, thereby enabling the detection of recurrent looping.

The sensor modules were built along with the data acquisition system and integrated into a proof-of-concept endoscopic test bench that uses a wire-pulley system to operate the endoscope tip, similar to that described in [21]. The pressure

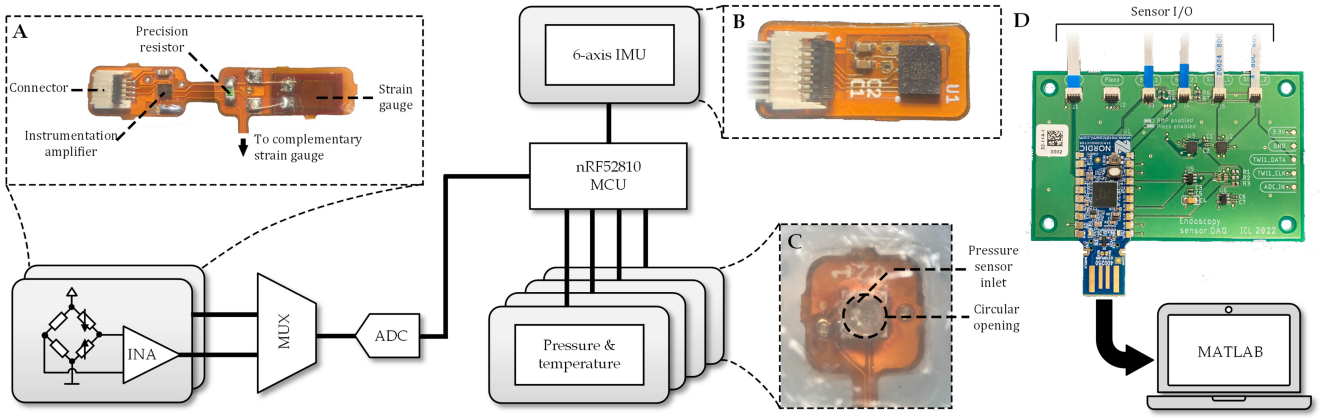

Fig. 2. System block diagram. a) The bending sensor PCB. The strain gauges are connected to an instrumentation amplifier in a half-bridge configuration. b) Inertial Measurement Unit (IMU) with a 3-axis accelerometer and a 3-axis gyroscope. c) A closeup image of the pressure sensor with the cushion attached on top d) The data acquisition (DAQ) card has a USB connector for connecting to the PC.

sensors were tested by placing a series of weights on them. Operation of the bending sensor modules was verified by programming the scope to maneuver in concentric loops and reading the sensor output. The effect of external temperature on the pressure and bending sensors was observed in a separate experiment. Operation of the IMU was verified by inserting the sensor through plastic tubing fixed in an alpha loop formation. Finally, the instrument was tested using a custom built colon phantom. Using a phantom instead of a live animal or human subjects was the clear choice at this point of device development. We can obtain sufficient data for a proof-of-concept study without the risks and cost of *in vivo* trials. The system is designed with off-the-shelf components with the aim of providing a low-cost solution and support the development of disposable colonoscope so as to minimize the risk of cross infection.

The combination of the sensing modalities has not previously been reported in colonoscopy. Furthermore, actual pressure values exerted to the colon wall have not been exhaustively reported before. In one study, the researches measured the forces associated with the insertion and twisting of the colonoscope, by adding strain sensors to the instruments handle [12]. Another study assessed the intraluminal pressures caused by insufflation. Here, air was pumped into the colon and the pump pressure was recorded [22]. The study found that a pressure of approximately 19 kPa could cause the sigmoid colon to rupture.

II. Methods

A. Sensor Selection

Our aim was to find compact, easy-to-use, and accurate sensors to use on the instrument. For the IMU we considered three of the largest manufacturers' products: BMI323 (Bosch Sensortec, Germany), ICM-42670-P (TDK InvenSense, Japan) and LSM6DSO (STMicroelectronics, Switzerland). These all have the same 12-lead footprint and are similarly priced and include both a 3-axis accelerometer and a 3-axis gyroscope. The power spectral densities for the accelerometer are 180, 100 and 70 $\mu g/\sqrt{Hz}$, respectively. The gyroscope angular rate spectral noise densities are 7, 7 and 3.8 $mdps/\sqrt{Hz}$, respectively. While not being the only factor accountable for the quality of the sensor, we chose the LSM6DSO as the IMU.

For the pressure sensor, we considered mainly three factors: resolution, pressure range, and package costruction. Especially the upper limit for absolute measurement range should be high enough to measure the pressures exerted to the colon wall. Here, we also examined three sensors: Bosch Sensortec BMP390, TDK InvenSense ICP-20100 and STMicroelectronics LPS22H series. The LPS22H outweighs the other two in both resolution (24-bit vs. 20-bit) and pressure range with the maximum pressure of 126 kPa versus 125 kPa for BMP390 and 110 kPa for ICP-20100. However, alternatively to the air cushion construction, we wanted to retain the ability to submerge the sensor to a silicone bulb, similar to [23], which the molded construction of the LPS22H does not allow. Our previous experience with the previous generations led us to choose the BMP390 [19].

The selection of the 350 Ω strain gauge BF350-3AA (generic) was done simply due to it's wide availability and low cost.

B. Sensor Module Fabrication

The sensors are housed on individual 0.2 mm thick flexible polyimide (PI) printed circuit boards (PCB). Each PCB has a flat flexible connector (FFC) to interface with the data acquisition card (DAQ). The pressure and bending sensor PCBs have meandering interconnects that connect the different parts of the PCB as shown in Figure 1b.

Each pressure sensor PCB houses two BMP390 absolute barometric pressure sensors. To allow the sensors to sense contact pressure, an air cushion is attached on top of each sensor. The PCB is shown in Fig. 2c. We had already used this approach to measure blood pressure from the fingertip [19]. The airtight pressure cushion made from low-density polyethylene (LDPE) is created by punching a hole to a silicone substrate with adhesive on both sides, and then attaching the air cushion to one side. By cutting a small opening to the air cushion, air is allowed to flow in the sensor cavity. This

TABLE I
COLLECTION OF THE POSSIBLE SENSORS CONSIDERED FOR THE DEVICE. THE SELECTED SENSORS ARE HIGHLIGHTED

Sensor type	Part ID	Manufacturer	Bit width	Details
Pressure	BMP390	Bosch Sensortec	20-bit	Max. 126 kPa
Pressure	ICP-20100	TDK InvenSense	20-bit	Max. 110 kPa
Pressure	LPS22H	STMicroelectronics	24-bit	Max. 125 kPa
IMU	BMI323	Bosch Sensortec	16-bit	180 $\mu g/\sqrt{Hz}$, 7 $mdps/\sqrt{Hz}$
IMU	ICM-42670-P	TDK InvenSense	16-bit	100 $\mu g/\sqrt{Hz}$, 7 $mdps/\sqrt{Hz}$
IMU	LSM6DSO	STMicroelectronics	16-bit	70 $\mu g/\sqrt{Hz}$, 3.8 $mdps/\sqrt{Hz}$
Strain	BF350-3AA	Generic	N/A	350 Ω

assembly is then attached to the sensor PCB. After assemble to the PCB, the air volume inside should remain constant and by applying force to the cushion, the internal pressure in the cavity can be sensed by the atmospheric pressure sensor. Two pressure sensor PCBs - a total of 4 sensors - are used on each joint of the endoscope in order to get a pressure reading from four directions. The scope is at its thickest (23 mm) around the pressure sensors, but due to the high conformity of the cushions, the diameter when inserted into the colon is 19 mm. The pressure sensor was also used to measure the temperature with its on-chip thermometer with a resolution of 16-bit/0.005 $°C/bit$.

The bending sensor PCB has two 350 Ω aluminium foil strain gauges. One module consists of two PCBs, each housing two strain gauges. The PCB is shown in Fig. 2a. The strain gauges are connected in a half bridge configuration with both strain gauges attached to the opposite sides of the endoscope. When the endoscope is bent, the strain gauge on one side will be stretched and the one on the other side will be compressed, doubling the sensing range and ensuring that the setup is partly protected from temperature variation. The strain gauges are connected to an instrumentation amplifier MAX41400 (Maxim Integrated) with a gain of 200 (G = 100 selectable). The reason for selecting the MAX41400 was its very small size (9-ball wafer level packaging) and suitability for medical equipment manufacturing. In addition, one of its intended use cases is to be used with a Wheatstone bridge strain gauge setup.

The IMU sensor board houses an LSM6DSO IMU. The assemled PCB is shown in Fig. 2b. In the current design, we only used one IMU placed at the tip of the endoscope.

C. Data Acquisition Electronics

A 4-layer DAQ card was designed to interface with the individual sensor boards. Nordic Semiconductor's nRF52840 based USB dongle is used as the main microcontroller unit (MCU). It hosts a 32-bit ARM Cortex-M4 processing unit and has built-in USB capabilities. The DAQ card has 4 or 6-pin FFC connectors for connecting the sensors - Two for the pressure sensor boards, two for the bending sensor boards and one for the IMU. The pressure sensors and the IMU are interfaced via SPI (Serial Peripheral Interface) and I^2C (Inter-Integrated Circuit) connections. An analog multiplexer (MAX4734, Maxim Integrated) is used to select between the two bending sensors. The amplified strain gauge signal is read via a 16-bit analog-to-digital converter (ADC). A low-dropout regulator (NCV8114, Onsemi) is used to generate a 1.65 V reference signal for the strain gauge instrumentation amplifier. The DAQ card is shown in Fig. 2d.

D. Endoscope Test Bench

A test bench system was built for sensor characterization. The system consists of a flexible endoscope shaft, housing a 9 mm instrument channel, a motorized capstan unit and control electronics. The control electronics is built based on the Arduino Uno R3 MCU platform and has an analog joystick and a pair of darlington motor controllers. The shaft is divided into a proximal part housing four Bowden cables, and a distal portion containing the sensing mechanics, which can be maneuvered in four directions by tightening the corresponding tendon via a pair of capstan drives. The capstan is driven by a 28BYJ-48 (generic) stepper motor, that is controlled with an analog joystick (KY-023, generic), enabling 2-DOF control of the endoscope tip. Additionally, the instrument can be programmed to trace a pre-defined trajectory. Figures 3a and b show the assembled system.

E. Effect of External Temperature

The actual measurement environment where the instrument is inserted into the human body differs from *in vitro* experiments. One such aspect is temperature. The measurements were done at room temperature, which is relatively low compared to body temperature. We studied the effect of external temperature on the sensors by placing the instrument in a heating chamber. The temperature was linearly increased from room temperature ($26°C$) to body temperature ($37°C$). We compared a pressure sensor equipped with and without the air cushion. In addition, the two bending sensors located in the same joint were compared: stressed and unstressed.

F. Software and Data Analysis

The firmware for the nRF52 MCU was written in C using Segger Embedded Studio. All sensors are sampled at 50 Hz. The sensor data (4 x pressure, 2 x bending, 6-axis IMU, temperature) along with the timestamp was sent via serial port connection to a PC running MATLAB R2022b. Each DAQ card is defined as a separate serial port object, so the theoretical limit for individual joints on the scope is 256. The sensor data plots can be read real-time from the GUI. The firmware for controlling the stepper motors for the

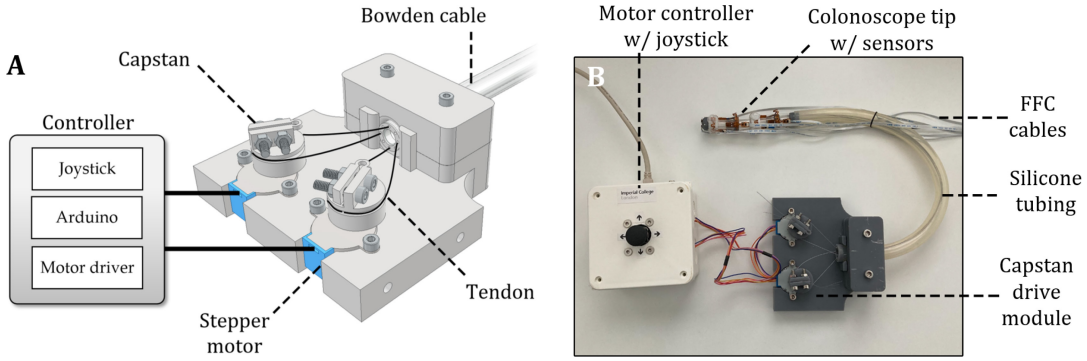

Fig. 3. Testbench design. a) Mechanics of the endoscope test bench. Four tendons are connected to a pair of capstans driven by stepper motors. The steel tendons are routed to the tip of the endoscope via bowden cables. The motors are controlled by a custom control unit with an analog joystick. b) Photograph of the test bench device with the sensor modules assembled.

endoscope test bench was built using the Arduino platform. All post-processing and data analysis was carried out using MATLAB R2022b. PCB design was done using Autodesk EAGLE 9.6.2 electronic design automation (EDA) software and mechanical design as well as finite element analysis (FEA) was done on Autodesk Inventor 2022 computer aided design (CAD) software. The 3D printing was done on a Formlabs Form 3 stereolithography (SLA) printer.

G. IMU Data Processing

Orientation of the scope tip was calculated using the gyroscope data fused with the accelerometer data using the Kalman filter. The resulting quaternion vector was sampled at 5 cm intervals. Since our device did not have pressure sensor modules at the proximal part of the instrument, we simulated the pressure sensor input by detecting the changes in the accelerometer signal. The same algorithm is directly applicable to the pressure sensors, since we know that the shaft was advanced in exactly 5 cm intervals. The insertion intervals were found from the accelerometer signal using a peak finding algorithm. Since we know that all tip advancements were exactly 5 cm, we can reconstruct every tip movement in a 3D plane. Orientation at each point is defined by a quaternion q and normalized (q_n):

$$q = a + b\mathbf{i} + c\mathbf{j} + d\mathbf{k} \tag{1}$$

where $\mathbf{i}$, $\mathbf{j}$ and $\mathbf{k}$ are the base vectors and a, b, c and d are real numbers outputted by the sensor fusion algorithm. Quaternion q and normalized (q_n):

$$q_n = \frac{q}{\sqrt{a^2 + b^2 + c^2 + d^2}} \tag{2}$$

We then define a vector u that points forward, e.g., to the direction of the Y-axis, in the sensor coordinate system. Vector u is converted to quaternion representation (u_q).

$$u = \begin{bmatrix} 0 \\ 1 \\ 0 \end{bmatrix} \cdot D \Leftrightarrow u_q = 0 + 0\mathbf{i} + D\mathbf{j} + 0\mathbf{k} \tag{3}$$

where D is the distance the scope advances at each interval ($D = 5$ cm). The scope advancement in 3D at each step is calculated by performing a rotation using the Hamilton product:

$$v_q = q u_q q^* \tag{4}$$

where q^* is the conjugate of quaternion q. Now, by appending each resulting $\mathbb{R}^3$ vector to the previous vector's endpoint, we get the 3D scope trajectory in the tube[24].

H. Colon Phantom

A partial colon phantom was fabricated to test the proposed sensor system *in vitro*. We used a 25.4 cm silicone bowel model (Chamberlain group, Massachusetts) with an inner diameter of 22 mm. The 3D printed supports were used to hold the model in place. Three different setups were assembled. The first assembly simulated a straight portion of the colon (Figure 5c). The second formed an S-shaped curve simulating the sigmoid colon. The sigmoid mesocolon was modeled by attaching a spring loaded fixture to the silicone tubing, simulating the resistance created by the mesentery (Figure 5d). For the third assembly, we added a sphincter model to create a narrowing in the tube (Figure 5e). This was achieved by flexible wiring wrapped across a 3D printed frame, and inserting the silicone tube through it. In order to protect the sensor electronics and minimize friction, the scope tip was first covered with a condom prior to being inserted into the colon model. A water-based lubricant was used to prevent damage to the silicone colon model.

We performed three types of experiments with the fabricated colon phantom. These are depicted in Figure 5c through e. For the first experiment, the silicone tube was set up as a straight pipe (Figure 5c). The endoscope was inserted 15 cm deep in the phantom. The scope tip was maneuvered to each four orthogonal direction (Figure 5a) while recording the contact pressure. Figure 5c shows the results of the experiment. For the second experiment, the silicone tube was arranged in an S-shape, simulating the sigmoid colon. It has been reported that 77% of the pain associated with colonoscopy happens when the scope tip is in the sigmoid colon [25]. The scope was inserted through the colon model and its bending was controlled with a joystick. Figure 5d shows the pressures from

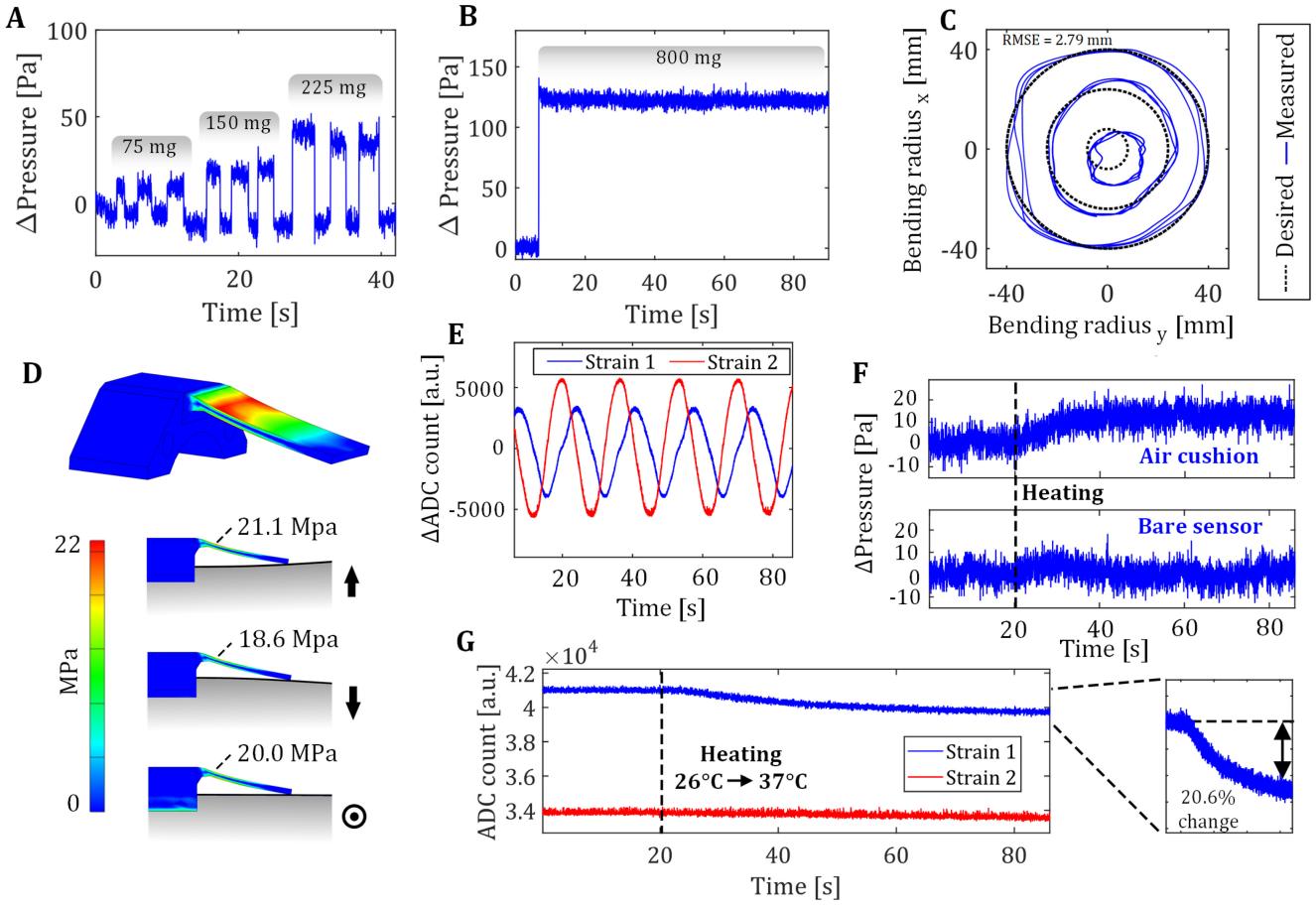

Fig. 4. Sensor characterization. a) Pressure sensor sensitivity was tested by placing weights on the sensor cushion. b) Step response and sensor drift was assessed by placing a weight on the sensor. c) The operation of the bending sensors was verified by programming the scope to move in concentric circles (r=10 mm, r=25 mm, r=40 mm) with the radius increasing at each step. The figure shows the desired and measured trajectories. d) Finite element analysis of the strain at the bending sensor plates at different bending directions. e) The endoscope tip was maneuvered in a circular trajectory, resulting in sinusoidal outputs. f) Effect of external temperature on the pressure sensors (with and without an air cushion). g) Effect of external temperature on the bending sensors in the same joint (x and y axes). Strain 1 is in a stressed state and strain 2 is unstressed, which causes the difference in their respective DC levels. Heating was turned on at approx. 20 s.

the distal pressure module (top) and the recorded strain from one of the bending sensors.

III. Results and Discussion

A. Sensor Characterization

1) Pressure Sensor: We measured the sensitivity of the pressure sensor modules by placing and removing very small weights (75 mg, 150 mg and 225 mg) on the pressure sensor cushion. The pressure output for the weights were 14.1 Pa, 30.8 Pa and 48.8 Pa respectively. The sensor was able to detect even the smallest weight and its loading and unloading cycle (Figure 4a). Because the weights used were so small, the adjacent unloaded pressure sensor was used to compensate for changes in atmospheric pressure. This was done by subtracting the unloaded pressure from the device under test. A 90 s measurement with the sensors unloaded resulted in atmospheric pressure fluctuating with mean and standard deviation (SD) of (102080 ± 3.4) Pa. Despite the compensation, there is some hysteresis present in the measurements. The result for the unloaded pressure showed a fluctuation with SD = 4.4 Pa. We believe that the hysteresis and drift are likely due to the small deformations of the cushion material between the loading and unloading cycles. A larger weight (800 mg) was used to see if there is any drift present. The initial overshoot was 6.8 Pa higher than the final value. It took 9.1 s for the pressure signal to settle to within 10% of the final value. As seen in Figure 4b there is very minimal drift noticeable and the step response is clearly sufficient in practice. It is notable, that the pressure changes reported above are very small in comparison with the pressures in the actual use case, where the expected pressures are measured in kilopascals versus pascals. For this reason, the amount of overshoot measured in the experiment is negligible.

Figure 4e shows, that when the heating is turned on, the pressure signal with air cushion equipped experiences a fast increase and stabilizes after that. The change in pressure is approximately 10 Pa. This can be considered negligible in a real use case. The bare pressure sensor does not experience the same effect. The phenomenon can be explained by the ideal gas law, since the increase in temperature causes the air inside the cushion to expand, thus increasing the pressure. The bare pressure sensor is not affected by this.

Characterization with actual pressure exerted in colonoscopy were observed in the colon model experiments.

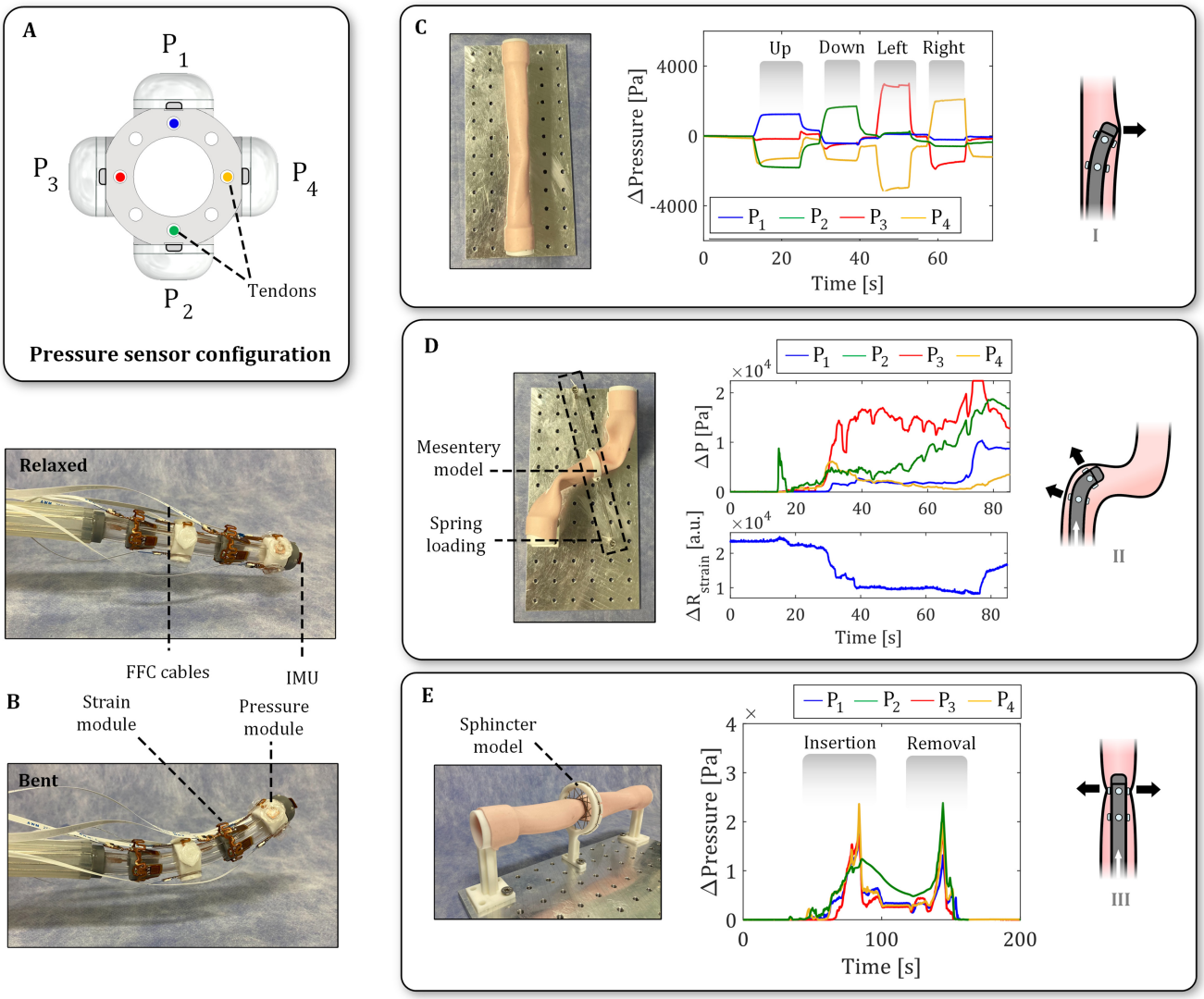

Fig. 5. Colon phantom experiments. a) Cross-section view of the scope with each tendon color coded. The plots in the figures correspond to the pressures associated with each tendon being pulled. b) Image of the endoscope tip in relaxed (top) and bent (bottom) positions. c) Straight tube with the scope tip maneuvered in four directions. d) The scope is advanced into the sigmoid colon model. The resistance of the sigmoid mesocolon is modeled via a spring-loaded fixture. e) A sphincter model is used to create a narrowing in the tube, similar to, e.g., the anal sphincter. Figures I-III depict the direction of forces associated with each experiment.

As can be seen from the pressure plot, P_3 shows the greatest increase when the scope is bent at approx. 30 s into the measurement. This happens due to the scope tip being pushed against the colon wall through the bend. After the bend, the scope is again straightened at approximately 75 s. For the third experiment, the silicone tube was again set up as a straight pipe and a sphincter model was placed halfway through the tube. When the scope was inserted through the sphincter model, relatively even pressure was exerted to all four pressure sensors. This is shown in Figure 5e. The pressure values in the colon phantom experiments range from approximately 1 kPa to 20 kPa.

2) Bending Sensor: The bending module has four plastic plates on which the strain gauges are placed. These are used to transfer the movement of the central silicone tube to the sensors. The plates are in a slightly stressed state when the scope is straight, and either relax or bend further when the scope is bent. Figure 4d shows the finite element analysis (FEA) of an individual plate being stressed. Perpendicular force exerted on the plate either increases or decreases the maximal Von Mises stress seen on the plate. The gauges are connected in a half-bridge configuration with the opposite sides stretching in opposite directions when the probe is bent. So each joint has two pairs of strain gauges in order to be able to record motion in a two-dimensional plane. The bending sensors had some variation in their output range, which can be seen in Figure 4f. Here, the endoscope tip was maneuvered in a circular trajectory, with the same tendon pulling ratio in both x and y directions, resulting in sinusoidal outputs. The same degree of bending resulted in slightly different changes in resistance in the sensors. Because of this, each sensor output had to be normalized. To get rid of the noise, a Butterworth low-pass filter with a cutoff frequency of 1 Hz was used to filter each signal. The variation could be partly caused by

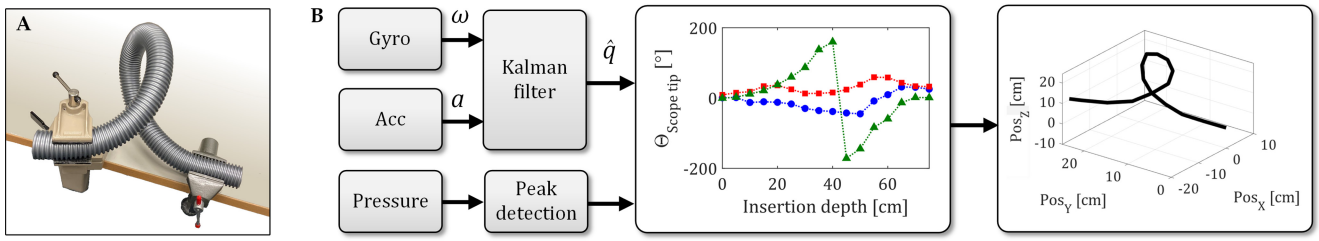

Fig. 6. IMU experiment. a) Plastic tubing fixed in an alpha loop formation. b) Sensor fusion algorithm for acquiring the three-dimensional scope tip trajectory. Angular velocity and acceleration are fused using the Kalman filter resulting in a quaternion describing the orientation of the scope tip. Insertion depth information acquired from the pressure sensors is combined with the orientation data and used to reconstruct a 3D path of the scope trajectory.

manufacturing tolerances in the inexpensive foil strain gauges, or the thickness of the glue used.

The operation of the calibrated bending sensors was verified by programming the scope to maneuver in certain trajectories. The tip was maneuvered in three concentric circular trajectories (r=10 mm, r=25 mm, r=40 mm) with the bending radius increasing at each step. These trajectories equal approximately the angles of 5°, 30° and 60° in relation to the proximal joint, respectively. Four full circles were done at each step. Figure 4c shows the results along with the desired trajectories. The root mean square error (RSME) of the measured and desired output was 2.79 mm. The error is a combination of both the inaccuracy of the sensors and the actuation itself. Variation in tightness of the tendons and any play in the motors can affect the actual movement of the scope.

Temperature variation affects the bending sensor readings significantly. In case of the stressed bending sensor, a decrease in the signal is caused by expansion of the gauges, which leads to change in resistance. Some of this effect is canceled due to the half-bridge configuration of the strain gauges, as both elements expand approximately the same amount. In the unstressed bending sensor, the temperature does not affect the signal as much and the change is only 37% of the one experienced by the stressed sensor.

In the colon model experiment, the tip of the scope was steered into the sigmoid colon. The corresponding bending sensor shows a decrease in strain gauge resistance as the endoscope tip turns. The strain then increases when the tip is straightened.

3) Inertial Measurement Unit: The estimation of position from the IMU data requires double integration of the acceleration signal, which leads to quadratic error propagation. Given the fact that there is significant drift, it is not feasible to get accurate 3D position solely from the inertial sensors [26]. Orientation detection, on the other hand, is much more accurate, since it only requires a single integration step, and, e.g., a Kalman filter to minimize gyroscope drift [27]. Insertion depth of the endoscope can be estimated from the pressure sensor outputs. As seen in Figure 5e, when the pressure module passes the anal sphincter, all four sensors show a spike in pressure. The sensor modules are placed on the scope shaft on 5 cm intervals, so we know the insertion depth of the scope shaft with a resolution of 5 cm. Since we can fairly accurately estimate orientation and we know the insertion depth of the endoscope, we can reconstruct the 3D trajectory of the instrument. Since the proof-of-concept device only has sensors in the scope tip, we demonstrated this by advancing the endoscope in 5 cm intervals through a plastic tubing. Figure 6a shows the setup with a 75 cm long tube with a 35 mm diameter representing an alpha loop formation.

IV. Conclusion

In this article, we proposed a multi-sensory system for sensing contact pressure, instrument bending and orientation. The system was designed and made using commercially available sensors, and the sensors are configured and refined for this specific application. A test bench system was built to verify the design, and the sensors are characterized with test bench. Finally, the design of the proposed sensing system was validated with a colon phantom. The experiments prove that the design is indeed viable for the use of colonoscopy. The next steps include integrating the proposed sensor technology into an colonoscope and validating the proposed with a more advanced colon model and clinical trials. The goal is to translate the proposed method for clinical use.

A. Challenges

Although the proposed system can provide the needed sensing capability for the endoscope, there were some issues with the design as well. Given the fact that the accelerometer and gyroscope exhibit drift, it is not feasible to get accurate 3D position solely from the inertial sensors [26]. We used the insertion depth data along with the orientation to reconstruct the 3D trajectory of the scope. However, this approach assumes that the tip is advanced the same amount each time, which is not often the case in real colonoscopy. So the method only provides a rough estimate of the trajectory of the scope. It is also possible to add an actuator to control the advancement of the scope as in [28]. This would enable high precision tracking of the insertion depth. Another issue we found was the effect of temperature variation to the bending sensor signal. Unlike in the case of a colon phantom, the actual use case involves the sensors to be exposed to substantial temperature changes, e.g., from room temperature of 20 $^{\circ}C$ to body temperature 37 $^{\circ}C$. Furthermore, the results show that the highest rate of change happens right after the heating is turned on and the effect of temperature is actually fairly small at body temperatures.

B. Translatability Into Clinical Practice

The current device is a proof-of-concept design, meant to showcase the capabilities of such platform in an *in vitro*

setting. In order for the technology to be applicable for clinical use, there are a couple of fundamental issues to be tackled. Firstly, in the prototype device the sensors and tendons are exposed in a way that would not be suitable for a clinical version. A flexible silicone sleeve molded around the tip of the instrument would provide protection for both the sensors and the patient. Secondly, the tethering solution for the individual sensor modules has to be iterated. Now all modules are individually powered and accessed via FFC cables, which results in a fairly large amount of cables. A possible solution would include daisy-chaining of the modules into a single bus with each module addressed individually with a unique identifier. Moreover, the cables are routed externally, which is not possible in a clinical version, which would require internal routing.

C. Future Directions

Controlling the elongated flexible colonoscope to avoid excessive contract pressure and looping is very challenging, especially when the endoscopist can only rely only on camera feedback. Each colon is different and even the most experienced clinician can face difficulties in inserting the colonoscope into the curved lumen. By introducing sensing onto the scope will aid the user in navigating through the colon and minimizing the risk on tearing and rupturing of the colon during colonoscopy [3], [4]. In addition to reducing the risk for life-threatening complications, we believe that minimizing the pain experienced can lift the stigma associated with colonoscopy, encouraging more people to get their colonoscopy which is a proven method to minimizing the risk of colorectal cancer [29], [30]. The proposed sensor system could also be useful for training physicians, e.g., in a simulated environment. Seeing which maneuvers produce excessive force or are prone to leading to loop formation, can be valuable in learning the best procedures. Altogether, the introduction of additional sensors to colonoscopy opens up opportunities for artificial intelligence (AI). AI has already shown remarkable potential especially in the field of radiology, where it is used as a complementary tool to aid the clinician. Currently in colonoscopy AI is mostly used for detecting lesions from the camera image [31], [32]. These approaches use convolutional neural networks (CNN), which have been successfully applied in image processing. However recent developments show promise toward AI being used in navigating the instrument and, e.g., assisting in biopsies [33]. A recent study proposed a three-layer model of autonomy in colonoscopy, ranging from manual robotic control to semi-autonomous operation, letting the operator to focus on important tasks [10]. The increasing levels of autonomy are an interesting direction of research - yet they cannot be achieved with traditional endoscopes. Accordingly, in the case of colonoscopy, we believe that rather than fully automating the procedure, AI is best used as an assistive tool by providing feedback to the user based on the multi-sensory inputs. One possible tool could be a real-time loop predictor that gives a warning when loop formation is probable. This would give the endoscopist time to adjust the manuever and prevent pain to the patient.

Author Contributions

Conception and design: T.P., B.G., S.I, B.L., System development: T.P. and B.G., Collection and assembly of data: T.P., Analysis and interpretation of the data: T.P., Drafting of the article: T.P., M.K. and B.L., All authors read and approved the final manuscript.

Data Availability

The data used and analysed during the current study is available from the corresponding author on reasonable request.

Conflict of Interest

The authors declare no conflict of interest.

References

[1] S. Ravindran et al., "National census of U.K. endoscopy services in 2019," *Frontline Gastroenterol.*, vol. 12, no. 6, pp. 451–460, 2021.
[2] H. Kavin, F. Sinicrope, and A. H. Esker, "Management of perforation of the colon at colonoscopy," *Amer. J. Gastroenterol.*, vol. 87, no. 2, pp. 451–460, 1992.
[3] A. J. Loeve, P. Fockens, and P. Breedveld, "Mechanical analysis of insertion problems and pain during colonoscopy: Why highly skill-dependent colonoscopy routines are necessary in the first place··· and how they may be avoided," *Can. J. Gastroenterol.*, vol. 27, no. 5, pp. 293–302, 2013.
[4] I. C. Roberts-Thomson and E. Teo, "Colonoscopy: Art or science?" *J. Gastroenterol. Hepatol.*, vol. 24, no. 2, pp. 180–184, 2009.
[5] A. Sivananthan, B. Glover, L. Ayaru, K. Patel, A. Darzi, and N. Patel, "The evolution of lower gastrointestinal endoscopy: Where are we now?" *Ther Adv. Gastrointest. Endosc.*, vol. 13, Dec. 2020, Art. no. 2631774520979591.
[6] S. D. Crockett, H. O. Cirri, R. Kelapure, J. A. Galanko, C. F. Martin, and E. S. Dellon, "Use of an abdominal compression device in colonoscopy: A randomized, sham-controlled trial," *Clin. Gastroenterol. Hepatol.*, vol. 14, no. 6, pp. 850–857, 2016.
[7] R. D. Pai, D. L. Carr-Locke, and C. C. Thompson, "Endoscopic evaluation of the defunctionalized stomach by using ShapeLock technology (with video)," *Gastrointest. Endosc.*, vol. 66, no. 3, pp. 578–581, 2007.
[8] C. W. Teshima, S. Zepeda-Gómez, S. H. AlShankiti, and G. S. Sandha, "Magnetic imaging-assisted colonoscopy vs conventional colonoscopy: A randomized controlled trial," *World J. Gastroenterol.*, vol. 20, no. 36, 2014, Art. no. 13178.
[9] J. W. Leung et al., "Magnetic endoscope imaging (ScopeGuide) elucidates the mechanism of action of the pain-alleviating impact of water exchange colonoscopy-attenuation of loop formation," *J. Intervent. Gastroenterol.*, vol. 2, no. 3, p. 142, 2012.
[10] J. W. Martin et al., "Enabling the future of colonoscopy with intelligent and autonomous magnetic manipulation," *Nat. Mach. Intell.*, vol. 2, no. 10, pp. 595–606, 2020.
[11] M. McCandless, A. Gerald, A. Carroll, H. Aihara, and S. Russo, "A soft robotic sleeve for safer colonoscopy procedures," *IEEE Robot. Autom. Lett.*, vol. 6, no. 3, pp. 5292–5299, Jul. 2021.
[12] M. N. Appleyard, C. A. Mosse, T. N. Mills, G. D. Bell, F. D. Castillo, and C. P. Swain, "The measurement of forces exerted during colonoscopy," *Gastrointest. Endosc.*, vol. 52, no. 2, pp. 237–240, 2000.
[13] S. Dogramadzi, G. Virk, G. Bell, R. Rowland, and J. Hancock, "Recording forces exerted on the bowel wall during colonoscopy: In vitro evaluation," *Int. J. Med. Robot. Comput. Assist. Surg.*, vol. 1, no. 4, pp. 89–97, 2005.
[14] J. Choi and D. Drozek, "Detection of looping during colonoscopy using bending sensors," *Open Med. Devices J.*, vol. 5, no. 1, pp. 1–7, 2013.
[15] A. O. Tal, J. Vermehren, and J. G. Albert, "Colon capsule endoscopy: Current status and future directions," *World J. Gastroenterol., WJG*, vol. 20, no. 44, 2014, Art. no. 16596.
[16] H. Liang, Y. Guan, Z. Xiao, C. Hu, and Z. Liu, "A screw propelling capsule robot," in *Proc. IEEE Int. Conf. Inf. Autom.*, 2011, pp. 786–791.
[17] L. Manfredi, L. Yue, J. Zhang, and A. Cuschieri, "A 4 DOFs variable stiffness soft module," in *Proc. IEEE Int. Conf. Soft Robot. (RoboSoft)*, 2018, pp. 94–99.

[18] S. S. Vedaei and K. A. Wahid, "MagnetOFuse: A hybrid tracking algorithm for wireless capsule endoscopy within the GI track," *IEEE Trans. Instrum. Meas.*, vol. 71, pp. 1–11, 2022.
[19] T. Panula, T. Koivisto, M. Pänkäälä, T. Niiranen, I. Kantola, and M. Kaisti, "An instrument for measuring blood pressure and assessing cardiovascular health from the fingertip," *Biosens. Bioelectron.*, vol. 167, Nov. 2020, Art. no. 112483.
[20] B. Maundy and S. J. Gift, "Strain gauge amplifier circuits," *IEEE Trans. Instrum. Meas.*, vol. 62, no. 4, pp. 693–700, Apr. 2013.
[21] W. Li, M. Shen, A. Gao, G.-Z. Yang, and B. Lo, "Towards a snake-like flexible robot for endoscopic submucosal dissection," *IEEE Trans. Med. Robot. Bion.*, vol. 3, no. 1, pp. 257–260, Feb. 2021.
[22] R. Kozarek, D. Earnest, M. Silverstein, and R. Smith, "Air-pressure-induced colon injury during diagnostic colonoscopy," *Gastroenterology*, vol. 78, no. 1, pp. 7–14, 1980.
[23] M. Kaisti et al., "Clinical assessment of a non-invasive wearable MEMS pressure sensor array for monitoring of arterial pulse waveform, heart rate and detection of atrial fibrillation," *NPJ Digit. Med.*, vol. 2, no. 1, p. 39, 2019.
[24] L. Vicci, "Quaternions and rotations in 3-space: The algebra and its geometric interpretation," Dept. Comput. Sci., Univ. North Carolina Chapel Hill, Chapel Hill, NC, USA, Rep. TR01-014, 2001.
[25] S. Shah, J. Brooker, C. Thapar, C. Williams, and B. Saunders, "Patient pain during colonoscopy: An analysis using real-time magnetic endoscope imaging," *Endoscopy*, vol. 34, no. 6, pp. 435–440, 2002.
[26] H. J. Luinge and P. H. Veltink, "Measuring orientation of human body segments using miniature gyroscopes and accelerometers," *Med. Biol. Eng. Comput.*, vol. 43, pp. 273–282, Apr. 2005.
[27] C. Kownacki, "Optimization approach to adapt Kalman filters for the real-time application of accelerometer and gyroscope signals' filtering," *Digit. Signal Process.*, vol. 21, no. 1, pp. 131–140, 2011.
[28] W. Li, Y.-Y. Tsai, G.-Z. Yang, and B. Lo, "A novel endoscope design using spiral technique for robotic-assisted endoscopy insertion," in *Proc. IEEE/RSJ Int. Conf. Intell. Robots Syst. (IROS)*, 2020, pp. 3119–3124.
[29] D. A. Lieberman et al., "Use of colonoscopy to screen asymptomatic adults for colorectal cancer," *New England J. Med.*, vol. 343, no. 3, pp. 162–168, 2000.
[30] A. Sonnenberg, F. Delco, and J. M. Inadomi, "Cost-effectiveness of colonoscopy in screening for colorectal cancer," *Ann. Internal Med.*, vol. 133, no. 8, pp. 573–584, 2000.
[31] D. Banik, K. Roy, D. Bhattacharjee, M. Nasipuri, and O. Krejcar, "Polyp-Net: A multimodel fusion network for polyp segmentation," *IEEE Trans. Instrum. Meas.*, vol. 70, pp. 1–12, 2020.
[32] G. Yue, S. Li, R. Cong, T. Zhou, B. Lei, and T. Wang, "Attention-guided pyramid context network for polyp segmentation in colonoscopy images," *IEEE Trans. Instrum. Meas.*, vol. 72, pp. 1–13, 2023.
[33] L. Introzzi, J. Zonca, F. Cabitza, P. Cherubini, and C. Reverberi, "Enhancing human-AI collaboration: The case of colonoscopy," *Digest. Liver Dis.*, vol. 56, no. 7, pp. 1131–1139, 2023.